A two-step synthesis of NaTaO3 microspheres for photocatalytic water splitting

ARTICLE *in* INTERNATIONAL JOURNAL OF HYDROGEN ENERGY · AUGUST 2014

Impact Factor: 3.31 · DOI: 10.1016/j.ijhydene.2014.03.023

4 AUTHORS, INCLUDING:

Yingxuan Li
Xinjiang Technical Institute of Physics & Ch…
34 PUBLICATIONS **492** CITATIONS
SEE PROFILE

Chuanyi Wang
Chinese Academy of Sciences
88 PUBLICATIONS **1,747** CITATIONS
SEE PROFILE

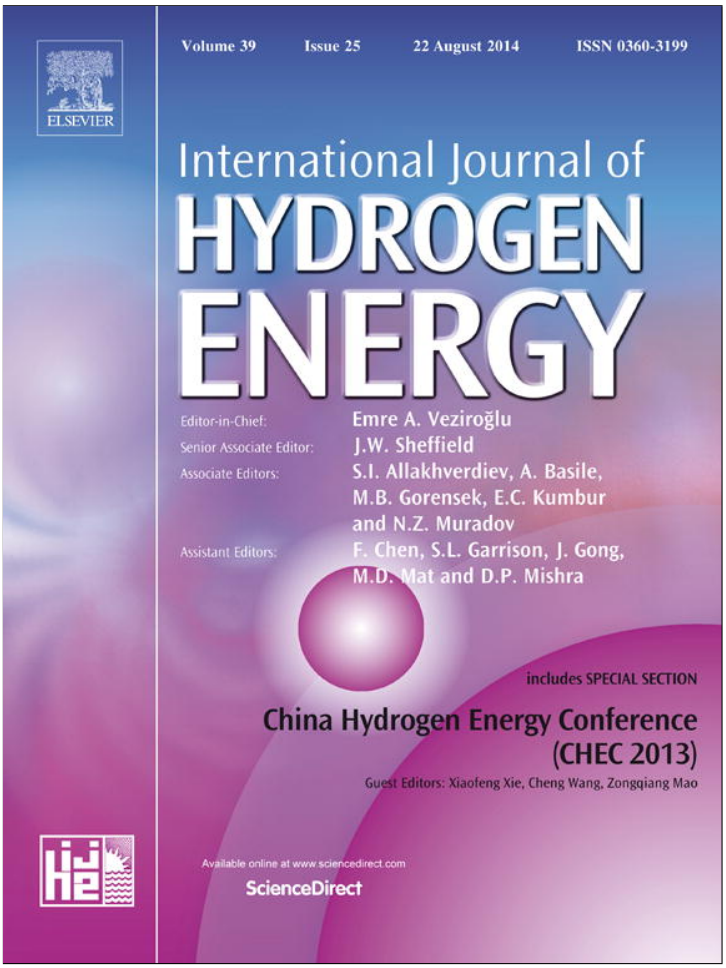

INTERNATIONAL JOURNAL OF HYDROGEN ENERGY 39 (2014) 13481–13485

Available online at www.sciencedirect.com

ScienceDirect

journal homepage: www.elsevier.com/locate/he

A two-step synthesis of $NaTaO_3$ microspheres for photocatalytic water splitting

Yingxuan Li [a], Huange Gou [b], Jianjiang Lu [b], Chuanyi Wang [a,*]

[a] Laboratory of Environmental Sciences and Technology, Xinjiang Technical Institute of Physics & Chemistry, Key Laboratory of Functional Materials and Devices for Special Environments, Chinese Academy of Sciences, Urumqi 830011, China

[b] School of Chemistry and Chemical Engineering, Shihezi University, Shihezi 832003, China

ARTICLE INFO

Article history:
Received 18 October 2013
Received in revised form
24 February 2014
Accepted 6 March 2014
Available online 13 April 2014

Keywords:
$NaTaO_3$
Microspheres
Photocatalytic water splitting
Rough surface

ABSTRACT

$NaTaO_3$ photocatalyst has been successfully synthesized by a two-step synthesis approach, namely, molten salt in combination with hydrothermal processing at a relatively low temperature. The key concept of the approach is using molten salt to convert Ta_2O_5 to a soluble Ta-precursor, and the aqueous solution of the obtained Ta-precursor is then transferred as a starting source of Ta to synthesize $NaTaO_3$ by a hydrothermal process. The obtained sample was characterized by powder X-ray diffraction (XRD), inductively coupled plasma emission spectrometry (ICP), field emission scanning electron microscopy (FESEM) and ultraviolet–visible (UV–vis) spectroscopy. A spherical morphology for $NaTaO_3$ has been observed by FESEM. Comparative study on hydrogen production from water splitting under UV-light irradiation evinces that the obtained sample exhibits more than 4 times higher photoactivity than its counterpart prepared by a solid state method. In addition, loading of NiO co-catalyst onto the surface of $NaTaO_3$ improves its efficiency for water splitting.

Introduction

Since the pioneering work of Honda and Fujishima [1], photocatalytic water splitting has been extensively studied due to its potential to produce clean and recyclable hydrogen energy [1–5]. Many metal oxides, such as titanates [6,7], niobates [8–11], and tantalates [12–14] have been developed as photocatalytic materials for water splitting. Among these materials, tantalates have been attracting great attention because tantalates possess conduction bands consisting of Ta5d orbitals locating at a more negative position than titanates (Ti3d) and niobates (Nb4d) [15]. Particularly, the quantum yield of $NiO/NaTaO_3$: La was estimated to be 56% at 270 nm, which is the highest quantum yield ever reported for photocatalysts in pure water splitting [16].

However, tantalates are usually synthesized by solid state methods at high temperature [14,17]. Recently, hydrothermal processing has also been applied to synthesize tantalates using tantalum oxide as a starting material [18,19]. To the best

* *Corresponding author*. Laboratory of Environmental Sciences and Technology, Xinjiang Technical Institute of Physics and Chemistry, Chinese Academy of Sciences, Urumqi, Xinjiang 830011, China. Tel.: +86 991 3835879; fax: +86 991 3838957.
E-mail addresses: yxli@ms.xjb.ac.cn (Y. Li), cywang@ms.xjb.ac.cn (C. Wang).

http://dx.doi.org/10.1016/j.ijhydene.2014.03.023

of our knowledge, the method for synthesizing tantalates is still very limited. The particle size, structure and morphology of the photocatalyst, which can be affected by the synthesis methods, play an important role in tuning their photocatalytic activity. Therefore, there has been much interest in exploring wet chemical approaches for the synthesis of tantalates, which might provide a potential route for fabricating tantalum based photocatalysts with novel morphologies and structures.

Herein, we report the synthesis of $NaTaO_3$ spherical assemblies by a two-step synthesis approach, namely, molten salt in combination with hydrothermal processing. The photocatalytic properties of the as-prepared samples for hydrogen generation under UV irradiation were investigated.

Materials and methods

Sample preparation

Ta_2O_5 (0.5 g), NaOH (3.855 g), and KOH (5.651) were loaded in a Teflon cup. The mixture was maintained at 240 °C for 20 h and air-cooled to room temperature. Next, deionized water (50 mL) was added into the cup. The solution was stirred for 30 min to dissolve the alkalis. The resulting suspension was centrifuged, and the solid product was collected and dissolved into 100 mL of deionized water to obtain a clear transparent solution. The solution (56 mL) was transferred into a 100 mL Teflon-lined stainless autoclave. Then NaOH aqueous solution (14 mL, 5 M) was slowly dropped into above clear solution under constant stirring. The autoclave was maintained at 180 °C for 2 h and air-cooled to room temperature. The solid product, denoted as $NaTaO_3$, was collected by centrifugation and washed thoroughly with deionized water, and finally dried at 60 °C under vacuum. As for NiO loading, the obtained $NaTaO_3$ was added into 5 mL of aqueous solution containing the required amount of $Ni(NO_3)_2$. The mixture was evaporated to dry solid and then calcined at 350 °C for 1 h to obtain NiO loaded $NaTaO_3$.

Characterization

The crystal phase properties of the samples were analyzed using a Bruker D8 X-ray diffractometer with Cu Kα radiation. The formula of $NaTaO_3$ was determined through inductively coupled plasma emission spectrometry (ICP; Perkin Elmer, Optima 5300DV) after the sample was dissolved in a mixture of HNO_3, and HF. Ultraviolet–visible (UV–vis) diffuse reflection spectra were recorded on a spectrophotometer (TU-1900), and $BaSO_4$ was employed as the internal reflectance standard. The morphology of the sample was examined using a field emission scanning electron microscopy (FESEM; ZEISS SUPRA55VP). The Brunauer–Emmett–Teller (BET) surface area measurements were recorded on a Quantachrome Autosorb-IQ-MP surface analyzer at liquid N_2 temperature (the sample was outgassed under vacuum at 200 °C for 2 h).

Photochemical reactions

Photocatalytic reactions were carried out in a closed gas-circulating system with a top quartz window. The light source used in the photocatalytic reactions is an 8 W bactericidal lamp with a maximum emission at 254 nm. In a typical experiment, 50 mg photocatalyst was dispersed in 80 mL of deionized H_2O at room temperature. The reaction system was evacuated several times to remove air prior to irradiation. The amount of produced gas was determined by an online gas chromatography (Agilent 7890A, TCD, N_2 carrier).

Results and discussion

The crystal structure of the synthesized sample was analyzed by XRD measurement (Fig. 1a). All of the diffraction peaks coincide with the $NaTaO_3$ phase (PDF 25-0863) with an orthorhombic structure [space group: (*Pcmn*)]. The inductively coupled plasma (ICP) was used to analyzed the composition of the prepared sample, showing that the molar ratio of K:Na:Ta is 0.01:0.96:1. The content of K in the product is so small that can be neglected. Therefore, the chemical formula of the prepared sample is concluded as $NaTaO_3$. The morphology of $NaTaO_3$ was examined by FESEM. As shown in Fig. 1b, the sample is composed of numerous microspheres with a diameter of 1–4 μm. A close view of the particles reveals that the sphere-like structure clearly indicates complete fusion (coalescence) of the particles. The coalescence and fusion process make the spheres to form larger particles. The SEM image of higher magnification (inset of Fig. 1b) confirms that

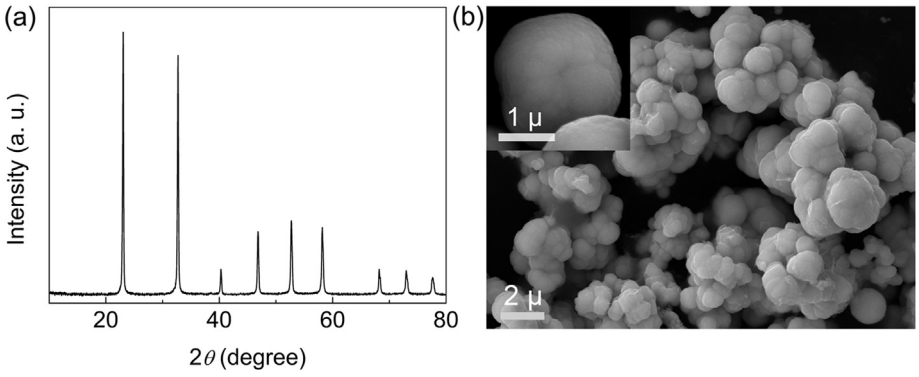

Fig. 1 – X-ray powder diffraction pattern (a) and SEM images (b) of the synthesized $NaTaO_3$. The upper inset of (b) is a typical FETEM image of an individual particle.

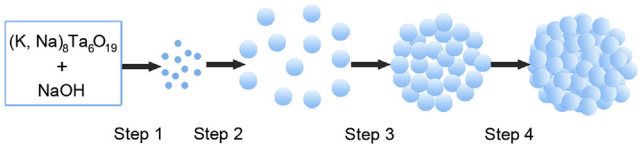

Scheme 1 – Schematical illustration of the proposed crystal growth of $NaTaO_3$ microspheres in the hydrothermal process.

the microsphere has a relatively rough surface composed of many tiny particles of diverse sizes. To our knowledge, this is the first report about the $NaTaO_3$ construction with secondary subunits at a relatively low temperature without using any templates or surfactants.

A possible formation process of the $NaTaO_3$ microspheres is schematically illustrated in Scheme 1. The involved reaction process can be described as follows:

$$Ta_2O_5 + (K, Na)OH \rightarrow (K, Na)_8Ta_6O_{19}\cdot nH_2O \quad (1)$$

$$(K, Na)_8Ta_6O_{19}\cdot nH_2O + NaOH \rightarrow (K, Na)TaO_3 \quad (2)$$

In the molten salt stage, soluble $(K, Na)_8Ta_6O_{19}\cdot nH_2O$ was obtained by the treatment of Ta_2O_5 in hydroxide melts at 240 °C for 20 h (Eq. (1)), as described previously [20]. During the following hydrothermal growth process, as shown in Scheme 1, four steps are involved. Firstly, $NaTaO_3$ nuclei are formed (Eq. (2)) when the concentration of Na^+ reaches or exceeds supersaturation (Step 1). Subsequently, as the reaction proceeds, $NaTaO_3$ nanocrystals are formed based on the Ostwald ripening mechanism (Step 2). The freshly crystalline nanoparticles are unstable and aggregated spontaneously into spherical structures to minimize their surface energy (Step 3). Afterward, the aggregates can not only act as centers for subsequent nanoparticle deposition, but also be further crystallized through Ostwald ripening. Therefore, with increasing reaction time, a compact aggregates can be achieved (Step 4). Moreover, in the hydrothermal conditions, the nucleation and aggregation growth of the $NaTaO_3$ crystals are kinetically fast, thus allowing the coalescence of the microspheres as shown in Fig. 1b.

For comparison, $NaTaO_3$ was synthesized by a traditional solid-state reaction approach according to the procedure previously reported [16]. The XRD pattern of the sample prepared by the solid-state method is shown in Fig. 2a. The diffraction peaks of the prepared sample match well with that of $NaTaO_3$, indicating that the synthesized product is of pure phase. SEM micrograph (Fig. 2b) shows that grains of the $NaTaO_3$ synthesized by the solid-state method possess cubic morphology with sharp edges. The side length with a large variation ranges from 0.2 to 1 μm.

The optical properties of the as-prepared samples were measured by UV–vis diffuse reflectance spectroscopy, which gives information on the electronic states of the semiconductor catalyst. Fig. 3 shows the UV–vis absorption spectra of $NaTaO_3$ cubes prepared by the solid-state method and hydrothermally prepared $NaTaO_3$ spheres. The reflection was transformed to absorbance intensity through the standard Kubelka–Munk method. The two samples exhibit similar absorption behavior with an absorption edge of 304 nm due to the band-gap transition. The band gap energy estimated from the onsets of the diffuse reflection spectra is about 4.08 eV.

The photocatalytic activity of the synthesized $NaTaO_3$ microspheres and microcubes for water splitting was performed under ultraviolet (UV) light irradiation (an 8 W bactericidal lamp), and the results were summarized in Table 1. Interestingly, the $NaTaO_3$ microspheres show much better photocatalytic performance than the $NaTaO_3$ prepared by the solid-state method (about 4 times higher), indicating the superiority of the two-step approach for the preparation of tantalate photocatalyst.

Generally, the photocatalytic activity of a material depends on many factors, such as crystallinity, surface area, and active sites [21]. Considering the treatment at the high temperature (1150 °C) for a long period (10 h), the crystallinity of $NaTaO_3$ synthesized by solid-state method should not be worse than that of $NaTaO_3$ microspheres. The surface areas of the two $NaTaO_3$ samples are shown in Table 1. A significant difference is that the surface area of $NaTaO_3$ microspheres (1.13 $m^2\ g^{-1}$) is much lower than that of $NaTaO_3$ prepared by solid-state method (2.18 $m^2\ g^{-1}$), which is reverse to the tested photoactivity. Therefore, based on the analysis above, the higher photocatalytic activity of $NaTaO_3$ microspheres is not due to the effects of crystallinity and specific surface area. There are

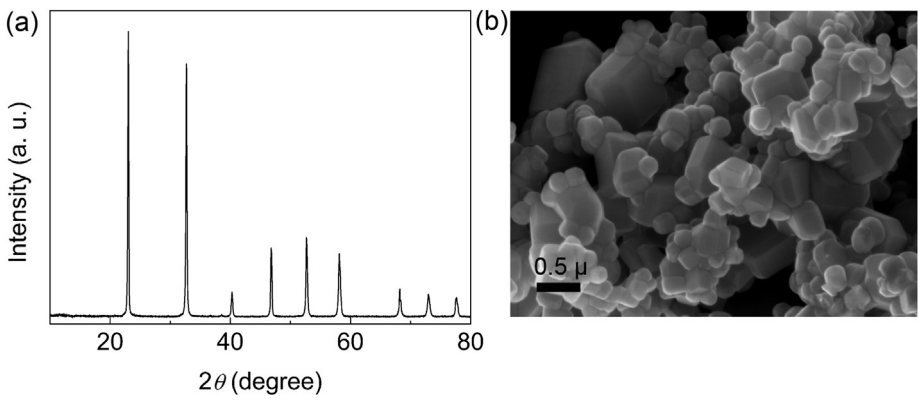

Fig. 2 – X-ray powder diffraction pattern (a) and the FETEM image (b) of the $NaTaO_3$ synthesized by a solid-state method.

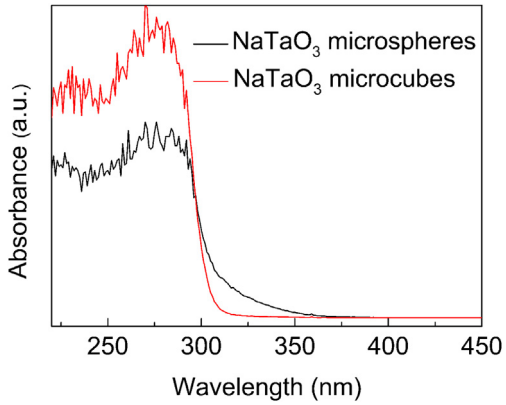

Fig. 3 – UV-vis diffuse reflectance spectra of $NaTaO_3$ samples.

other factors that can contribute to the photocatalytic performance of $NaTaO_3$ microspheres.

The photocatalytic water splitting process with semiconductors includes two steps [22]. First, under light irradiation, electrons are injected from the valence band to the conduction band of the semiconductor, resulting in the formation of electrons and holes. Second, the photoinduced charges migrate to the surfaces of particles to reduce and oxidize the surface adsorbed water to produce H_2 and O_2, respectively [22]. According to this mechanism, the photocatalytic activity is closely related to the separation of electron–hole pairs and the adsorption of H_2O molecules at the catalyst surface.

As observed by the SEM measurements, the $NaTaO_3$ microspheres (Fig. 1b) have a rough surface, while the surface of $NaTaO_3$ synthesized by solid-state method appears smooth (Fig. 2b). The presence of rough surface might be beneficial for the enhancement of photocatalytic activity when considering the following two factors. First, compared with $NaTaO_3$ cubes with flat surface, there are more favorable binding sites for the attachment of H_2O molecules on the rough surface of $NaTaO_3$ microspheres [23]. Second, for $NaTaO_3$ microspheres, many boundaries among $NaTaO_3$ nanoparticles might be helpful for H_2O adsorption and the separation of photogenerated electron–hole pairs. Therefore, the superior photocatalytic performance of $NaTaO_3$ microspheres with rough surface is easily understandable in terms of the increases in the available amounts of the photogenerated charges and adsorbed water by rough surface.

In order to improve the photoactivity, NiO co-catalyst was loaded onto the surface of the $NaTaO_3$ microspheres. The amount of the NiO co-catalyst was varied from 0 to 0.40 wt%. Fig. 4a shows the correlation of H_2 evolution with the amount of NiO loading. In the presence of NiO co-catalyst, photocatalytic activity is remarkably enhanced. As seen from Fig. 4a, the optimum concentration of NiO-loading is 0.3 wt%, whereas further increase or decrease of NiO loading leads to decreased photocatalytic performance. The time dependence of the amounts of H_2 and O_2 evolutions on 0.3 wt% NiO–$NaTaO_3$ microspheres in overall water splitting is shown in Fig. 4b. During the experimental period, both H_2 and O_2 evolved stoichiometrically and steadily.

Table 1 – Surface areas and photocatalytic rates for hydrogen production of $NaTaO_3$ samples.

Sample	BET surface area ($m^2\ g^{-1}$)	Activity ($\mu mol\ h^{-1}$)	
		H_2	O_2
$NaTaO_3$ microspheres	1.13	0.26	–
$NaTaO_3$ microcubes	2.18	0.05	–

Conclusions

In summary, $NaTaO_3$ microspheres were successfully prepared by a two-step synthesis at a relatively low temperature. The as-obtained sample shows promising activity in overall water splitting under UV-light irradiation. Its H_2 evolution rate is 4 times higher than that of $NaTaO_3$ prepared by a solid-state method. This is tentatively attributed to the efficiently enhanced separation of photogenerated charge carriers and favorable adsorption of H_2O molecules due to the rough surface of the $NaTaO_3$ microspheres. NiO has been used as co-catalyst to modify the photocatalytic activity of the $NaTaO_3$ microspheres. The photocatalyst with 0.3 wt% NiO loading gives the highest activity. This work not only provides an example of shape-dependent photoactivity of the $NaTaO_3$ crystals but also opens new possibilities to design ideal building blocks of tantalate materials for the applications in advanced photocatalysis.

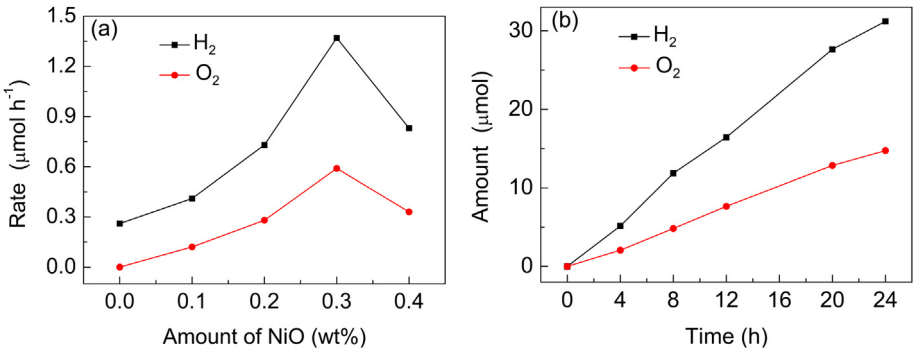

Fig. 4 – (a) Influence of the loading of the NiO co-catalyst on the activity of $NaTaO_3$ microspheres. (b) Photocatalytic overall water splitting at 0.3% NiO–$NaTaO_3$ microspheres under UV-light irradiation.

Acknowledgments

This work was financially supported by the Excellent Youth Foundation of Xinjiang Uygur Autonomous Region (2013711004), National Nature Science Foundation of China (Grant Nos. 21001113, 21173261), the "One Hundred Talents Project Foundation Program" of Chinese Academy of Sciences, International Science & Technology Cooperation Program of Xinjiang Uygur Autonomous Region (20126017), the CAS "Western Action Plan" (KGZD-EW-502), the "Cross-Cooperation Program for Creative Research Teams" of Chinese Academy of Sciences, and the "Western Light" Program of Chinese Academy of Sciences (YB201303).

REFERENCES

[1] Honda K, Fujishima A. Electrochemical photolysis of water at a semiconductor electrode. Nature 1972;238:37–8.
[2] Wang X, Xu Q, Li M, Shen S, Wang X, Wang Y, et al. Photocatalytic overall water splitting promoted by an α-β phase junction on Ga_2O_3. Angew Chem Int Ed 2012;51:13089–92.
[3] Li YX, Chen G, Zhou C, Sun JX. A simple template-free synthesis of nanoporous ZnS-In_2S_3-Ag_2S solid solutions for highly efficient photocatalytic H_2 evolution under visible light. Chem Commun; 2009:2020–2.
[4] Li Y, Chen G, Zhou C, Li Z. Photocatalytic water splitting over a protonated layered perovskite tantalate $H_{1.81}Sr_{0.81}Bi_{0.19}Ta_2O_7$. Catal Lett 2008;123:80–3.
[5] Zou Z, Ye J, Sayama K, Arakawa H. Direct splitting of water under visible light irradiation with an oxide semiconductor photocatalyst. Nature 2001;414:625–7.
[6] Hwang DW, Lee JS, Li W, Oh SH. Electronic band structure and photocatalytic activity of $Ln_2Ti_2O_7$ (Ln = La, Pr, Nd). J Phys Chem B 2003;107:4963–70.
[7] Li Q, Kako T, Ye J. Facile ion-exchanged synthesis of Sn^{2+} incorporated potassium titanate nanoribbons and their visible-light-responded photocatalytic activity. Int J Hydrogen Energy 2011;36:4716–24.
[8] Li Y, Chen G, Zhang H, Lv Z. Band structure and photocatalytic activities for H_2 production of $ABi_2Nb_2O_9$ (A = Ca, Sr, Ba). Int J Hydrogen Energy 2010;35:2252–6.
[9] Yan L, Zhang J, Zhou X, Wu X, Lan J, Wang Y, et al. Crystalline phase-dependent photocatalytic water splitting for hydrogen generation on $KNbO_3$ submicro-crystals. Int J Hydrogen Energy 2013;38:3554–61.
[10] Hosogi Y, Shimodaira Y, Kato H, Kobayashi H, Kudo A. Role of Sn^{2+} in the band structure of SnM_2O_6 and $Sn_2M_2O_7$ (M = Nb and Ta) and their photocatalytic properties. Chem Mater 2008;20(4):1299–307.
[11] Hu Y, Guo P, Guo L. Synthesis and photocatalytic properties of Cr-doped $KSr_2Nb_3O_{10}$ for hydrogen production. Int J Hydrogen Energy 2012;37:1007–13.
[12] Kanhere P, Zheng J, Chen Z. Visible light driven photocatalytic hydrogen evolution and photophysical properties of Bi^{3+} doped $NaTaO_3$. Int J Hydrogen Energy 2012;37:4889–96.
[13] Iwase A, Kato H, Kudo A. The effect of Au cocatalyst loaded on La-doped $NaTaO_3$ on photocatalytic water splitting and O_2 photoreduction. Appl Catal B Environ 2013;136–137:89–93.
[14] Sun JX, Chen G, Li YX, Jin RC, Wang Q. Novel (Na, K)TaO_3 single crystal nanocubes: molten salt synthesis, invariable energy level doping and excellent photocatalytic performance. Energy Environ Sci 2011;4:4052–60.
[15] Zhang G, Jiang W, Yu S. Preparation, characterization and photocatalytic property of nanosized K-Ta mixed oxides via a sol-gel method. Mater Res Bull 2010;45:1741–7.
[16] Kato H, Asakura K, Kudo A. Highly efficient water splitting into H_2 and O_2 over lanthanum doped $NaTaO_3$ photocatalysts with high crystallinity and surface nanostructure. J Am Chem Soc 2003;125:3082–9.
[17] Li Y, Zang L, Li Y, Liu Y, Liu C, Zhang Y, et al. Photoinduced topotactic growth of bismuth nanoparticles from bulk $SrBi_2Ta_2O_9$. Chem Mater 2013;25:2045–50.
[18] Xu TG, Zhang C, Shao X, Wu K, Zhu YF. Monomolecular-layer $Ba_5Ta_4O_{15}$ nanosheets: synthesis and investigation of photocatalytic properties. Adv Funct Mater 2006;16:1599–607.
[19] Xu T, Zhao X, Zhu YF. Synthesis of hexagonal $BaTa_2O_6$ nanorods and influence of defects on the photocatalytic activity. J Phys Chem B 2006;110:25825–32.
[20] Li Y, Chen S, He H, Zhang Y, Wang C. Tuning activities of $K_{1.9}Na_{0.1}Ta_2O_6{\cdot}2H_2O$ nanocrystals in photocatalysis by controlling exposed facets. ACS Appl Mater Interfaces 2013;5:10260–5.
[21] Xu H, Reunchan P, Ouyang S, Tong H, Umezawa N, Kako T, et al. Anatase TiO_2 single crystals exposed with high-reactive {111} facets toward efficient H_2 evolution. Chem Mater 2013;25:405–11.
[22] Li Y, Liu H, Wang C. Nanostructured sulfides: synthesis and applications in hydrogen generation. Curr Inorg Chem 2012;2:168–83.
[23] Yoon TJ, Youn Y-S, Son W-S, Seo B, Ahn KH, Lee Y-W. Dimensionless entropy of fusion as a simple criterion to predict agglomeration in the supercritical antisolvent process. Cryst Growth Des 2013;13:3481–9.